Heliyon 6 (2020) e04986

Contents lists available at ScienceDirect

Heliyon

journal homepage: www.cell.com/heliyon

Research article

Acenaphtoquinoxaline as a selective fluorescent sensor for Hg (II) detection: experimental and theoretical studies

Mahdieh Darroudi [a,**], Ghodsi Mohammadi Ziarani [a,*], Jahan B. Ghasemi [b], Alireza Badiei [b]

[a] Department of Chemistry, Faculty of Physic and Chemistry, Alzahra University, Tehran P.O. Box 1993893973, Iran
[b] School of Chemistry, College of Science, University of Tehran, Tehran, Iran

ARTICLE INFO

Keywords:
Chemical sensor
Optical spectroscopy
Density functional theory
Green chemistry
Organic synthesis
Molecular modeling
Environmental chemistry
Water chemistry
Acenaphtoquinoxaline
Quinoxaline-based receptor
Fluorescence
Sensor
Hg^{2+} ion

ABSTRACT

A new fluorescent chemosensor based on quinoxaline was successfully synthesized through a facile and green catalytic reaction of *ortho*-phenylenediamine (*O*-PDA) and acenaphthylene-1,2-dione in the presence of SBA-Pr-SO_3H. Prepared a "*switch-off*" quinoxaline-based receptor to recognized Hg^{2+} ion in high selectively and, without any interference from other metal ions, was developed. The photophysical behavior of this fluorophore was studied in acetonitrile by using fluorescence spectra. The fluorescence properties of several cations to acenaphtoquinoxaline were investigated in acetonitrile, and the competition test displayed that the probe fluorescence changes were specific for Hg^{2+} ion. The obtained results have shown high selectivity and sensitivity only for Hg^{2+}. Also, the detection limit was as low as 42 ppb, and a top linear trend was observed between the concentration of Hg^{2+} ions and fluorescence intensity. The binding stoichiometry between chemosensor **L** and Hg^{2+} was found to be 1:1. Moreover, a computational study was performed to obtain an electronic description of the fluorescence emission and quenching mechanisms. The optimized structures and binding mechanisms were supported with a high correlation and agreement by spectroscopy and DFT calculations.

1. Introduction

Quinoxaline moiety, as an attractive building block, has been widely applied as a ubiquitous motif in pharmaceuticals [1, 2, 3, 4, 5]. Mainly, quinoxaline displays potential antibacterial, antiprotozoal, antiviral, anti-inflammatory, and kinase-inhibitory properties [6, 7, 8, 9]. This scaffold is also utilized as electroluminescent materials, cavitands, organic semiconductors, dyes, and chemically controllable switches [10, 11, 12]. Additionally, it could be used as the electron-withdrawing group for intramolecular charge transfer in push-pull structures due to highly π-deficient aromaticity [13, 14, 15]. Detection and removal of heavy metals and toxic materials are pivotal from environmental points of view [8,10,16, 17, 18, 19, 20, 21]. The ionophore moiety contains nitrogen atoms that have an affinity for soft metal, including Hg^{2+} ion [22]. It is expected that the electron density of the fluorophore moieties can be reduced through the effect of an electron-withdrawing coordinated cation. Also, remarkable changes in the absorption spectra and fluorescence intensity should be raised by the complexation of ionophore to metal ion [23,24].

The pollution of heavy metal ions possesses violent risks for the environment and human health. Due to the high risk of water contamination and to the conservation of the environment, water quality monitoring is a contemporary concern. The pollution of heavy metal ions possesses violent risks for the environment and human health. Due to the high risk of water contamination indicating environmental protection, water quality monitoring is a contemporary concern [14,15]. Thus, the development of novel, highly sensitive, and selective chemosensors for the convenient and rapid detection of metal ions is considerably increased. The design and synthesis of highly selective sensors for metal ion in the aqueous or non-aqueous media have been received much attention as an active area of research, exclusively, fluorescent sensors are a rapidly developing field of research [25, 26, 27, 28, 29, 30], which have gained significant attention because of their exciting features as high reversibility, specificity, and sensitivity [31,32]. A chemosensor fluorophore is immensely demanded in terms of economic viewpoint [33, 34, 35]. Among various toxic metal ions, Hg^{2+} is vital due to its biological significance as well as its adverse influence on living organisms [36, 37, 38, 39]. On the other hand, Understanding of the detrimental effects of

* Corresponding author.
** Corresponding author.
E-mail addresses: M.darroudi@Alzahra.ac.ir (M. Darroudi), gmohammadi@Alzahra.ac.ir (G. Mohammadi Ziarani).

https://doi.org/10.1016/j.heliyon.2020.e04986
Received 22 July 2020; Received in revised form 23 August 2020; Accepted 16 September 2020

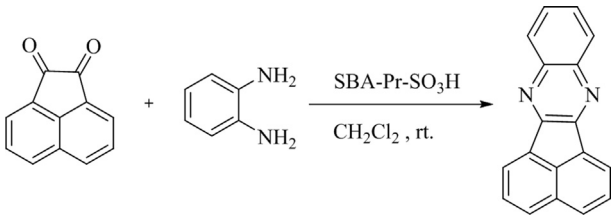

Scheme 1. Synthetic route of acenaphtoquinoxaline.

Hg^{2+} ion exposure has sparked interest in the progress of new tools for detecting Hg^{2+} ion in the environment. As a heavy metal ion, mercury is notorious as a highly poisonous and precarious ion, but it is still employed in various anthropological, agricultural, and industrial activities [40, 41, 42, 43, 44]. These collectively have led to the urgent development of an efficient and appropriate chemosensor for Hg^{2+} metal ion that is capable of detecting this ion in environmental and biological samples in the presence of other interfering ions. Mostly, the Hg^{2+} is commonly known to effectively quench the receptor fluorescence through its efficient spin-orbit coupling [39,45, 46, 47]. In recent years, more and more Hg^{2+} fluorescent sensors have been developed due to their rapidity, high sensitivity, and selectivity. However, some prepared sensors have much more detection limit to Hg^{2+} ion detection in high sensitivity, most of these receptors are difficult to prepare, or the reactions are not cost-effective. Herein, we prepared a fluorescent sensor by organic synthesis, which has some superior as simple operation, low-cost starting material, avoiding by-product, high yield, and in short reaction time [48, 49, 50, 51, 52, 53, 54, 55, 56, 57, 58, 59, 60, 61, 62, 63, 64, 65, 66].

As a part of our ongoing research on the design of fluorescent probes for ions [41,43,67, 68, 69, 70, 71, 72], a novel acenaphtoquinoxaline containing fluorescent probe was designed and synthesized through acidic mesoporous catalyst SBA-Pr-SO_3H and also examined for ion detection compared to other chemical receptors. Furthermore, the computational studies implementing DFT calculations were used to justified the experimental observations for probable binding modes studies.

2. Experimental

2.1. Materials and instruments

All the commercial-grade chemicals and metal salts in the analytical grade were used without further purifications. Stock solutions of metal ions (Ba^{2+}, Ca^{2+}, Cd^{2+}, Cs^{+}, Co^{2+}, Cr^{3+}, Fe^{3+}, Fe^{2+}, Hg^{2+}, K^{+}, Li^{+}, Mg^{2+}, Mn^{2+}, Na^{+}, Ni^{2+}, Sr^{2+}, and Zn^{2+}) were prepared using their nitrate salts purchasing from Merck company.

The Infrared spectra (IR) of the sample was recorded from the KBr disc by Fourier-Transform (FT-IR) Burker Tensor 27 instrument. The melting point of the sample was measured through the capillary tube method with an Electrothermal 9200 device. All the fluorescence measurements (PL) were recorded on a Cary Eclipse fluorescent spectrometer (Agilent Technologies, USA) equipped with a fluorescence 10 nm quartz cell (Ex Slit:5.0 nm; Em: 10.0 nm; PMT Voltage:650V) at room temperature.

2.1.1. SBA-Pr-SO_3H preparation

The SBA Pr-SO_3H was synthesized as reported articles [73, 74, 75]. The experimental method was demonstrated in the Supporting Information file.

2.1.2. Synthesis of acenaphtoquinoxaline

To a solution of *ortho*-phenylenediamine (1 mmol) in dichloromethane (5 ml), acenaphthylene-1,2-dione (1 mmol), and 0.02 g catalyst SBA-Pr-SO_3H were added. The solution was stirred at room temperature, and the progress of the reaction was monitored by TLC. The reaction mixture was filtered to recover the catalyst, and the filtrate evaporated under the vacuum to obtain the crude product, which is recrystallized from ethanol to give pure acenaphtoquinoxaline at a high yield 99% (Scheme 1) [76].

MP: 237–239 °C, ^{1}H NMR (400 MHz, $CDC1_3$): 8.21 (d, 2H, J = 6.8 Hz), 8.02 (dd, 2H, J = 6.2, 3.2 Hz), 7.90 (d, 2H, J = 8.4 Hz), 7.65 (t, 2H, J = 7 Hz), 7.57 (dd, 2H, J = 6.4, 3.6 Hz); ^{13}C NMR (100 MHz, $CDC1_3$): 155.19, 142.39, 137.60, 132.92, 131.10, 130.47, 130.59, 130.36, 129.78, 122.96; IR (KBr): 3443, 3047, 2922, 2361, 1614, 1481 cm^{-1}

2.1.3. Ligand preparation

Acenaphtoquinoxaline (254.3 mg, 1 mmol) as a ligand was dissolved in CH_3CN (10 ml) to have a stock solution (1×10^{-1} mol L^{-1}). The stock

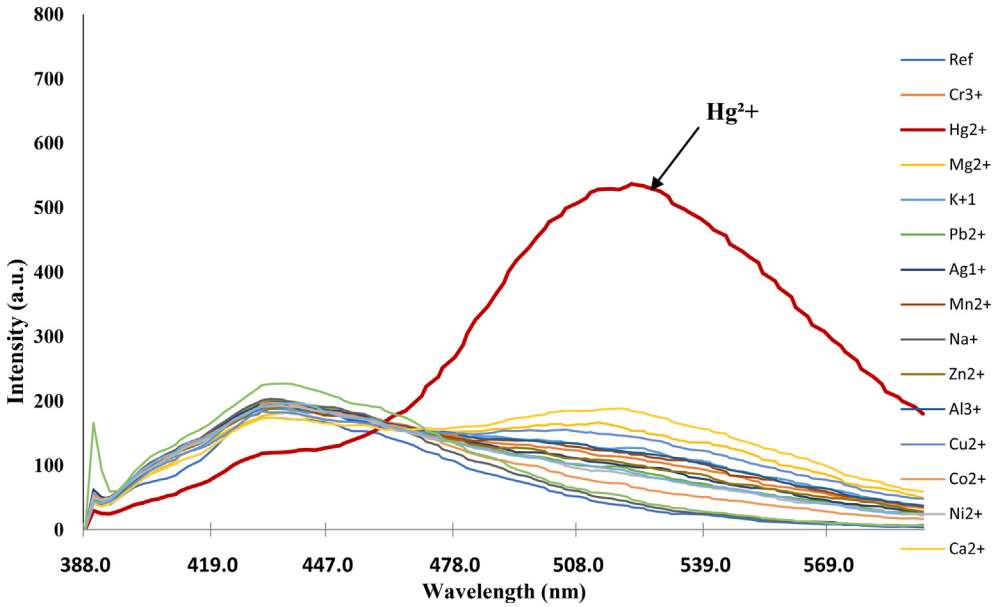

Figure 1. Fluorescence spectra of acenaphtoquinoxaline (2.5 ml, 0.001 M) after the addition of different cations (100μL, 0.001 M) with λ_{ex} at 380 nm.

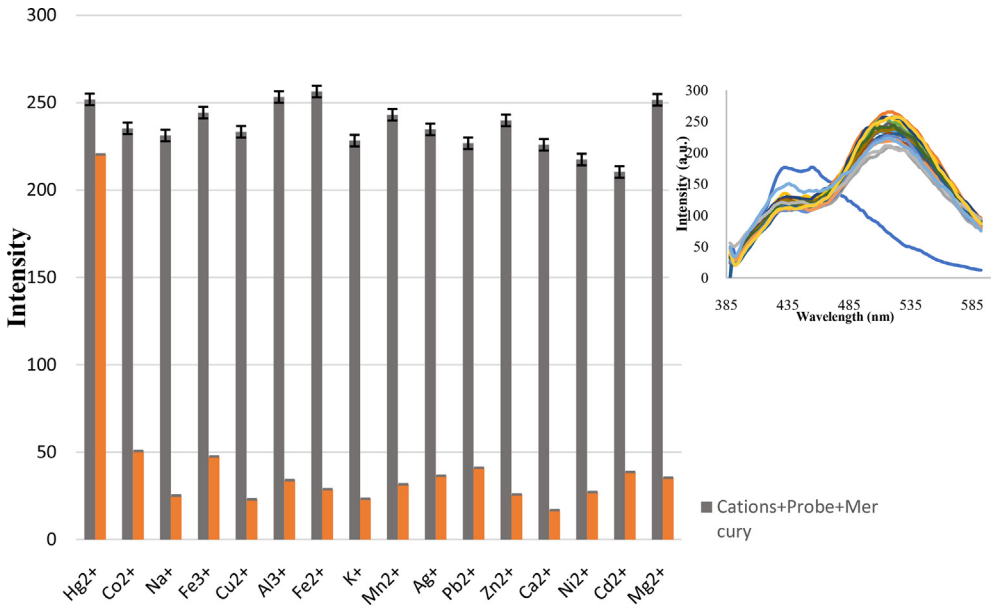

Figure 2. The effect of interfering ion on the emission of (100μL, 0.001 M) Hg^{2+} ion, and inset: Fluorescence emission spectra of acenaphtoquinoxaline solution (2.5 ml, 0.001 M) after addition of various cations (100μL, 0.1 M) with λ_{ex} at 380 nm n = 3, Sd_{avrage} = 2.13.

solution (1×10^3 μL) was diluted to acetonitrile (100 mL) to prepare the final concentration (1×10^{-3} mol L^{-1}).

2.1.4. Metal-salt solution preparation

The stock solutions of a various metal salt such as Ba^{2+}, Ca^{2+}, Cd^{2+}, Cs^{+}, Co^{2+}, Cr^{3+}, Fe^{3+}, Fe^{2+}, Hg^{2+}, K^{+}, Li^{+}, Mg^{2+}, Mn^{2+}, Na^{+}, Ni^{2+}, Sr^{2+}, and Zn^{2+} (1×10^{-2} mol L^{-1}) were prepared by dissolving a suitable amount of nitrate salts in double-distilled pure water.

2.1.5. Fluorescence studies

The experiment was performed in acetonitrile as a solvent at 25 ± 1°C, and before recording any spectrum, sufficient time was given to ensure the solution uniformity. Florescence measurement of acenaphtoquinoxaline (1×10^{-3} mol L^{-1}) was evaluated by adding aliquots of metal salts solution (1×10^{-2} mol L^{-1}) with the excitation wavelength at 385 nm, and emission spectra were recorded in the range 385–600 nm. For cation sensing experiments, 100 μl of each ion (1×10^{-2} mol L^{-1}) mixed with the ligand acenaphtoquinoxaline **L** solution (2.5 mL), which were used for fluorescence measurement. Among all studied metal ions, only mercury ion could impose fluorescent intensity of ligand acenaphtoquinoxaline, as shown in Figure 1. However, upon the Hg^{2+} addition, a strong redshift is observed, while the other ions affect slightly.

2.1.6. Titration

To monitor the fluorescence property of ligand, prepared acenaphtoquinoxaline (2.5 mL, 1×10^{-3} mol L^{-1}) was transferred into a quartz cell, then an incremental amount of Hg^{2+} solution from 0 to 400 μL (1×10^{-4} mol L^{-1}) was added to the resulting suspension. The fluorescence spectra were recorded after 3 min at room temperature.

2.1.7. Adverse cations

The adverse effects of other cations were studied by addition of a certain amount of cation solution (1×10^{-3} mol L^{-1}, 100 μL) individually to a suspension mixture of Hg^{2+} ion (100 μL) and acenaphtoquinoxaline (2.5 ml, 1×10^{-3} mol L^{-1}). After adequately mixing and enough resting to reach equilibrium, the fluorescence spectra were recorded.

2.1.8. Computational

To gain more insights about the electronic properties of the Hg^{2+}-ligand complex, the acenaphtoquinoxaline and acenaphtoquinoxaline-cation geometries were optimized by the DFT calculation in the solution state [77, 78, 79]. These calculations were corresponded to specious with B3LYP/6–311++G(2d,p) level of theory. The solvent effect is considered by using of CPCM calculations in acetonitrile [80, 81, 82, 83]. In this investigation, we used a simple approach to provide a semi-quantitative explanation for experimental results. The reported energies are Gibbs free energies, including zero-point vibrational corrections, entropy, and thermal corrections at 298 K. Moreover, to obtain more accuracy in our calculations, all energies were corrected with dispersion effect using the DFT-D2 method of Grimme [84]. The essential frontier molecular orbitals (FMO) was used for explaining the concerning charge transfer for acenaphtoquinoxaline.

3. Results and discussion

3.1. Synthesis acenaphtoquinoxaline

The classical method for synthesis of quinoxaline involves the reaction of *O*-PDA with acenaphthylene-1,2-dione using SBA-Pr-SO_3H as nanocatalyst in the dichloromethane at room temperature condition with good yield and short reaction time (Scheme 1).

3.2. Fluorescent response to cations

The detecting metal cation ability of acenaphtoquinoxaline could be evaluated in acetonitrile by fluorescence response toward a wide range of cations including Ba^{2+}, Ca^{2+}, Cd^{2+}, Cs^{+}, Co^{2+}, Cr^{3+}, Fe^{3+}, Fe^{2+}, Hg^{2+}, K^{+}, Li^{+}, Mg^{2+}, Mn^{2+}, Na^{+}, Ni^{2+}, Sr^{2+}, and Zn^{2+}, which are capable of changing the fluorescence spectrum of acenaphtoquinoxaline (Figure 1). It was instantly recorded after adding cations to the ligand upon excitation at 310 nm. Acenaphtoquinoxaline represents an intense emission band at 385 nm. However, upon the Hg^{2+} ion addition, a redshift in the fluorescence emission band is observed at 520 nm; while the other cations affect the emission spectrum barely.

3.3. Interfering cations

The proposed method's selectivity was investigated through the study of the effect of the consistent mixtures of target metal ion and common interfering cations on the emission spectrum of chemosensor (Figure 2).

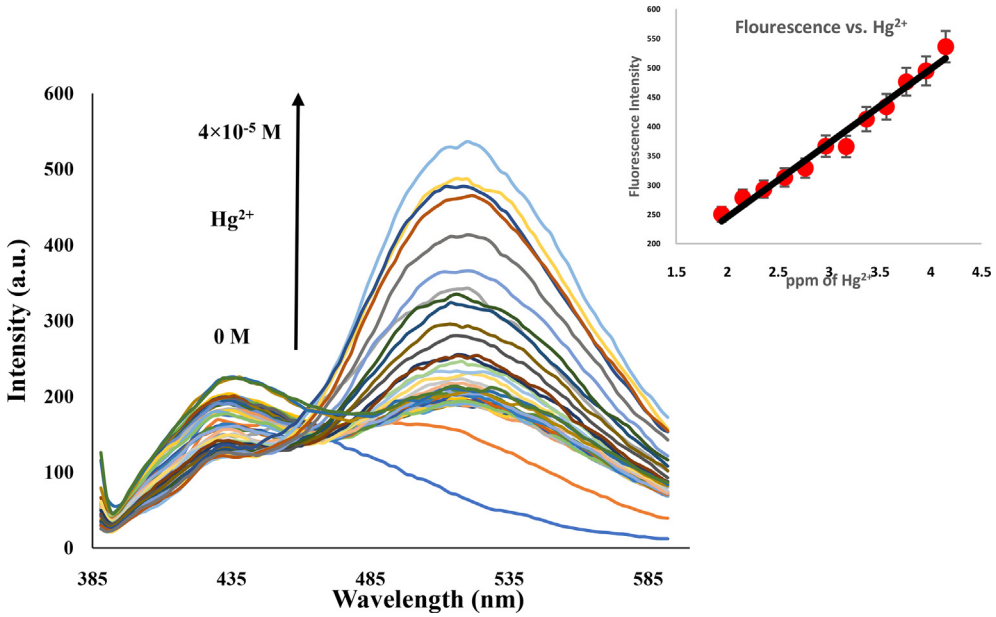

Figure 3. Fluorometric titration of acenaphtoquinoxaline (2.5 ml, 0.001 M) Hg^{2+} ion aqueous (10–400 μL, 0.0001 M), inset: the relationship between the emission maximum intensity λ_{em}520 nm and concentration of Hg^{2+}. n = 3, SD $_{avrage}$ = 1.79.

Generally, the emission spectra of acenaphtoquinoxaline solution were monitored in the presence of Hg^{2+} ion and higher amounts of competing cations. In the presence of other cation species, the Hg^{2+} ion created a significant redshift in the fluorescent emission of acenaphtoquinoxaline.

In order to determine the influence of other metal ions on the fluorescent detection of Hg^{2+} in CH_3CN, Ba^{2+}, Ca^{2+}, Cd^{2+}, Cs^{+}, Co^{2+}, Cr^{3+}, Fe^{3+}, Fe^{2+}, Hg^{2+}, K^{+}, Li^{+}, Mg^{2+}, Mn^{2+}, Na^{+}, Ni^{2+}, Sr^{2+}, and Zn^{2+} (0.001 M) were added to the acenaphtoquinoxaline solution (0.1 M) with Hg^{2+} (0.0001 M). The interfering ions induced small or no tangible changes in the fluorescence intensity of the chemosensor. As a result, the acenaphtoquinoxaline can be considered as a highly selective and reliable chemosensor for Hg^{2+} ion detection.

3.4. Titration experiments

For evaluation of the quantitative interaction between chemosensor and Hg^{2+}, a titration experiment was performed (Figure 3).

By increasing concentration Hg^{2+} ion from 0 to 0.004 M, the fluorescence intensity was constant at 435 nm, but the intensity linearly increased at 520 nm (inset in Figure 3). The results indicated that the stoichiometry ratio of Hg^{2+} to the ligand is 1:1. The linear equation of fluorescence intensity vs. Hg^{2+} ppm was;

$$Y = -6.8(\pm 17.8) + 126.2(\pm 5.7) \times Cppm$$

at 520 nm as emission wavelength. Furthermore, the detection limit calculated based on the above equation as the signal of the blank was -6.8 + 3×17.8, and the calculated detection limit was 42 ppb. Fluorescence redshift by the addition of Hg^{2+} metal ion could be explained through the heavy metal effect or due to its large size and low tendency towards a covalent bond with an N-donor. Moreover, the high sensitivity toward the Hg^{2+} ion is possibly owing to high affinity and fast chelating kinetics with a nitrogen group on the ligand acenaphtoquinoxaline.

3.5. Reusability

Addition of 1 Equiv. Na_2S restores the fluorescence of the sensor back to the baseline level at 520 nm. It is found that sulfide ion also decreased the fluorescence intensity of the L-Hg^{2+} ensemble in concentration dependence. This sensor displays high sensitivity to sulfide ion to form the stable species, which may be attributed to the high affinity of Hg^{2+} toward S^{2-}, such that it binds effectively with sulfide ion and sulfur-containing compounds. The formation constant for HgS is high; hence the probe-Hg2+ ensemble prefers to bind with sulfide. The sensor can also be recovered, but the process (Figure 4).

3.6. Electronic characterization

Electronic characterization methods suggest one of the most reliable data about the chemical structure of different molecules. In order to understand the reactivity of reactants and charge transfer, FMO analysis was performed for the acenaphtoquinoxaline (Ligand) and Ligand-Metal (Hg^{2+}) in an organic environment at B3LYP/6-311+G(d,p) level. The HOMO and LUMO energies band gap play a pivotal role in determining the stability, electrical and chemical reactivity, and optical properties. The HOMO term is defining as the highest occupied molecular orbital with donating capability. Contrary, the LUMO term defining as the lowest unoccupied molecular orbital indicates the electron-accepting ability due to lower energy and deficiency of electrons. The conjugated structures are characterized by the HOMO-LUMO band gap, which is the result of intermolecular charge transfer (ICT). The ICT occurred through a π-conjugated path from the donor group to the efficient acceptor group.

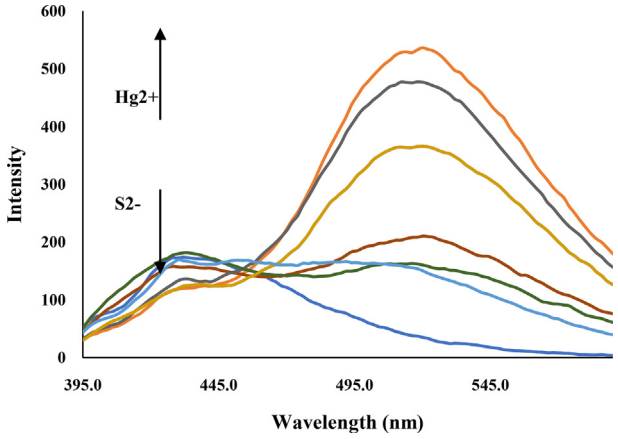

Figure 4. Fluorescence response of Acenaphtaquinoxaline-Hg^{2+} ensemble to S^{2-}.

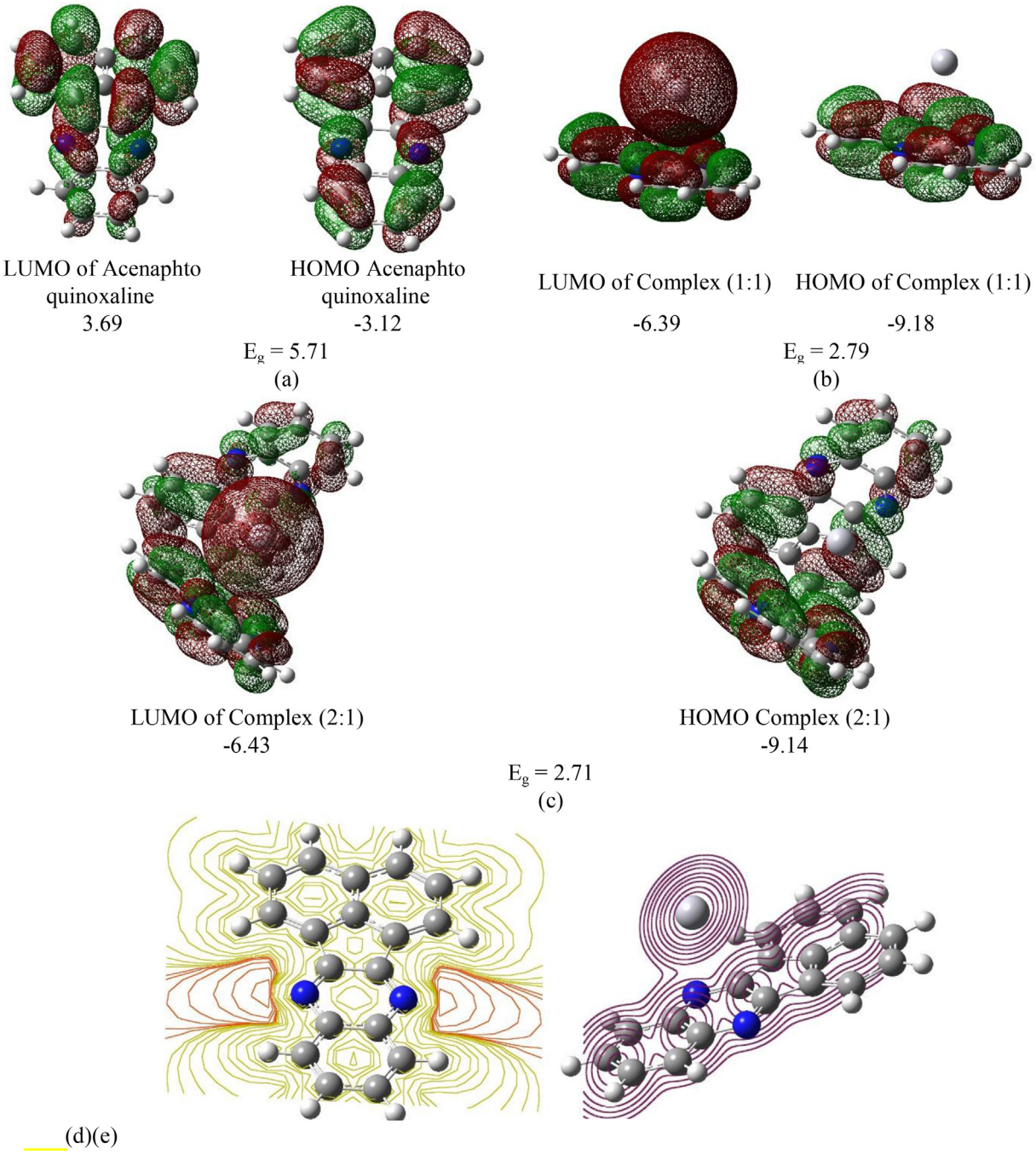

Figure 5. The HOMO and LUMO energies and the electronic bandgap (E_g) in eV for the lowest energy for (a) Acenaphto quinoxaline, (b) Complex (1:1), (c) Complex (2:1) (e) SCF acenaphtoquinoxaline and (f) SCF of Complex (1:1).

3.7. Mulliken charge analysis

Mulliken charge analysis was done through the calculation of the electron population for an individual atom. In receptor **L**, the positive charge was found at C11, C12, C14, and C15. The positive charge for these carbon atoms is because of the presence of electronegative N atoms in the closest sites. The N13, N16 atoms have negative charges; also, some C atoms in the receptor acenaphtoquinoxaline possess a negative charge. MEP is associated with electron density and is a very suitable descriptor in acceptor sites for the nucleophilic and electrophilic attack as hydrogen bonding interactions. The negative electron density localized on the N atoms. Furthermore, C11, C12, C14, and C15 have positive potential because of the N atom. The acenaphtoquinoxaline molecule has some potential spots for the nucleophilic and electrophilic attack.

The HOMO-LUMO energy gap presented the charge transfer interactions occurring inside the ligand. The metal complexes structures, **CL1**, and **CL2** were predicted using the DFT method to gain a better understanding of the ICT, which took place between metal ion and receptor during complexation. The optimized structure of ligand acenaphtoquinoxaline was shown in Figure 5, where the acenaphtoquinoxaline provided a pseudo cavity of two N atoms as a donor to form a complex with Hg^{2+} ion. Moreover, the bandgap of HOMO and LUMO of receptor **L** becomes smaller for C-**L1** and C-**L2** complexes. The decreasing bandgap energy was observed because of the

Table 1. The changes in binding energy ϵ, enthalpy and Gibbs free energy in kJ mol.

Entry	ΔE	ΔH	ΔG
(1:1) complex	-295.8	-304.6	-253.6
(2:1) complex	-279.9	-287.5	-233.9

Table 2. The calculated chemical hardness η, global electrophilicity ω, global nucleophilicity N, and global softness indices s, in eV, for Probe Quinoxaline, (1:1) complex and (2:1) complex.

Entry	ω	η	s	N
Probe Quinoxaline	0.006	13.62	0.07	0.29
(1:1) complex	10.88	5.57	0.17	0.07
(2:1) complex	11.19	5.41	0.18	0.07

charge transfer, which occurred between the acenaphtoquinoxaline and the Hg^{2+} ion of the complex excited state (C-**L**1 and C-**L**2).

The HOMO-LUMO energy of acenaphtoquinoxaline was -3.12 eV and 3.69 eV, respectively, and the gap between HOMO and LUMO is 6.81 eV (Figure 5). Also, the HOMO and LUMO of acenaphtoquinoxaline-C-**L**1 ions were -9.18 eV and -6.39 eV, and for another plausible complex of C-**L**2 was -9.14 eV and -6.43 eV, respectively. In other words, the energy gap of HOMO-LUMO of acenaphtoquinoxaline was much higher than metal ion complexes structures ($\Delta E_{gap} = 6.81 > 2.79 > 2.71$ eV). It was noted that the HOMO of the complex in the 1:1 stochiometric is the most stabilized level of energy than other molecular forms, whereas the complex in 2:1 stoichiometric ratio has the most stable HOMO-LUMO gap energy. These molecular orbitals related to the electronic transition for acenaphtoquinoxaline and the charge transfer can occur from acenaphtoquinoxaline to Hg atom. A comparing of low-value $E_{H\text{-}L}$ of C-**L**1 and C-**L**2 complexes to **L** suggests a significant effect of charge transfer. The molecular structure aromatic part of acenaphtoquinoxaline are planer with strong fluorescence and the relevant HOMO, and LUMO of acenaphtoquinoxaline was localized mainly on the electron donor fluorene and the benzene ring of quinoxaline structure, whereas the LUMO level is predominantly situated on the N, N-six membered ring conjugated to the benzene and partly located on the aromatic region. After Hg^{2+} addition, the molecular structure of complex C-**L**1 and C-**L**2 is formed, and at the same time, it can be seen that the LUMO of complexes is mostly localized on the Hg^{2+} atom, and the HOMO-LUMO band gap forming the C-**L**1 complex is 2.79 eV. The bandgap of the complex is remarkably lower than that of the ligand acenaphtoquinoxaline, which indicated the existence of a stable complex. The potential SCF spin density plot counters are presented in Figure 5, show the density is situated on N, N′-6 membered ring toward Hg^{2+} ion. It was consistent with the contribution of metal d orbitals to the orbitals involved in the charge transition. Molecular orbitals were mostly populated by metal d orbitals of Hg, and a ligand to metal charge transfer was observed.

In order to demonstrate a comparison between the stability of **L**-Hg^{2+} complexes, the corresponding binding energies are listed in Table 1. It is shown that a stronger interaction between the **L** and Hg^{2+} metal ion in the C-**L**1 complex was observed, and also binding energy decreased for (2:1) complex. So, it can be predicted that C-**L**1 should be regarded as the most favorable interaction.

Further, the energies of HOMO and LUMO are used to describe the stability, reactivity, and charge transfer through global indices. The electronic chemical potential is defined as the mean value of HOMO and LUMO energies as $\mu \sim (\varepsilon_{HOMO}+\varepsilon_{LOMO})/2$ and global electrophilicity, which establish the ratio $\omega = \mu^2/(2\eta)$ of the charge transfer process. Chemical hardness is the difference of HOMO and LUMO energies as $\eta = (\varepsilon_{LUMO}\text{-}\varepsilon_{HOMO})$, global softness index computed as $S = 1/2\eta$, and global nucleophilicity index, which is based on HOMO energies, defined as differences between HOMO of species and HOMO of tetracyano ethylene (TCE) ($N = \varepsilon_{HOMO(molecule)}\text{-}\varepsilon_{HOMO(TCE)}$) [85, 86, 87, 88].

To recognize that the origin of charge transfer during the reaction, global properties for acenaphtoquinoxaline and mercury ion is shown in Table 2.

Global nucleophilicity and electrophilicity index and electron chemical potential value could be used to describe the charge transfer (electron releasing and accepting ability of molecule). The highest relative global nucleophilicity value is found to be 0.29 eV in the ligand acenaphtoquinoxaline as obtained results. Moreover, the highest amount of global electrophilicity is found to be 11.19 e.V in the **L**-Metal complex in (2:1) ratio C-**L**2. Generally, the chemical hardness and chemical softness of ligand and metal are found to be 0.07, 0.17, and 0.18 eV, respectively, which is considered as a reactive compound (Table 2).

4. Conclusions

In summary, acenaphtoquinoxaline-based turn-off fluorescent ligand was successfully synthesized through a facile reaction through a short-time reaction between *o*-PDA and acenaphthylene-1,2-dione with the excellent yield for the visual detection of Hg^{2+} ion in the CH_3CN solution using the fluorescence spectroscopy. The system is a highly selective and sensitive fluorescent Hg^{2+} sensor over a variety of metal ions. Furthermore, excellent linearity was observed between the concentration of Hg^{2+} and the fluorescence intensity variation with the detection limit of 42 ppb. It is expected that this work will enhance and improve the development of the fluorescent chemosensors by heteroatoms, which could be used for various practical applications in different chemical and environmental systems. Moreover, the Hg^{2+} ion sensing mechanism through the intramolecular charge transfer was investigated by DFT calculations. The experimental and computational results could be used for the development of many chemosensors.

Declarations

Author contribution statement

Mahdieh Darroudi: Conceived and designed the experiments; Performed the experiments; Analyzed and interpreted the data; Contributed reagents, materials, analysis tools or data; Wrote the paper.

Ghodsi Mohammadi Ziarani, Alireza Badiei: Contributed reagents, materials, analysis tools or data; Wrote the paper.

Jahan B. Ghasemi: Analyzed and interpreted the data; Wrote the paper.

Funding statement

This research did not receive any specific grant from funding agencies in the public, commercial, or not-for-profit sectors.

Competing interest statement

The authors declare no conflict of interest.

Additional information

No additional information is available for this paper.

Acknowledgements

We gratefully acknowledge the financial support from the Research Council of Alzahra University and the University of Tehran. The numerical calculations reported in this paper were fully performed at SANCAR, Turkish-German University System, and Nodes of Computational Applications and Research.

References

[1] H.M. Loughran, Z. Han, J.E. Wrobel, S.E. Decker, G. Ruthel, B.D. Freedman, R.N. Harty, A.B. Reitz, Quinoxaline-based inhibitors of ebola and marburg VP40 egress, Bioorg. Med. Chem. Lett 26 (2016) 3429–3435.

[2] M. Hajri, M.A. Esteve, O. Khoumeri, R. Abderrahim, T. Terme, M. Montana, P. Vanelle, Synthesis and evaluation of in vitro antiproliferative activity of new ethyl 3-(arylethynyl)quinoxaline-2-carboxylate and pyrido[4,3-b]quinoxalin-1(2H)-one derivatives, Eur. J. Med. Chem. 124 (2016) 959–966.

[3] P. Corona, A. Carta, M. Loriga, G. Vitale, G. Paglietti, Synthesis and in vitro antitumor activity of new quinoxaline derivatives, Eur. J. Med. Chem. 44 (2009) 1579–1591.

[4] A. Jaso, B. Zarranz, I. Aldana, A. Monge, Synthesis of new quinoxaline-2-carboxylate 1,4-dioxide derivatives as anti-Mycobacterium tuberculosis agents, J. Med. Chem. 48 (2005) 2019–2025.

[5] L.E. Seitz, W.J. Suling, R.C. Reynolds, Synthesis and antimycobacterial activity of pyrazine and quinoxaline derivatives, J. Med. Chem. 45 (2002) 5604–5606.

[6] Y.B. Kim, Y.H. Kim, J.Y. Park, S.K. Kim, Synthesis and biological activity of new quinoxaline antibiotics of echinomycin analogues, Bioorg. Med. Chem. Lett 14 (2004) 541–544.

[7] W. He, M.R. Myers, B. Hanney, A.P. Spada, G. Bilder, H. Galzcinski, D. Amin, S. Needle, K. Page, Z. Jayyosi, M.H. Perrone, Potent quinoxaline-based inhibitors of PDGF receptor tyrosine kinase activity. Part 2: the synthesis and biological activities of RPR127963 an orally bioavailable inhibitor, in: Bioorganic Med. Chem. Lett., Elsevier Ltd, 2003, pp. 3097–3100.

[8] S. Tariq, K. Somakala, M. Amir, Quinoxaline: an insight into the recent pharmacological advances, Eur. J. Med. Chem. 143 (2018) 542–557.

[9] Z. Zhao, W.H. Leister, R.G. Robinson, S.F. Barnett, D. Defeo-Jones, R.E. Jones, G.D. Hartman, J.R. Huff, H.E. Huber, M.E. Duggan, C.W. Lindsley, Discovery of 2,3,5-trisubstituted pyridine derivatives as potent Akt1 and Akt2 dual inhibitors, Bioorg. Med. Chem. Lett 15 (2005) 905–909.

[10] K.R. Justin Thomas, M. Velusamy, T. Lin Jiann, C.H. Chuen, Y.T. Tao, Chromophore-labeled quinoxaline derivatives as efficient electroluminescent materials, Chem. Mater. 17 (2005) 1860–1866.

[11] S. Dailey, W.J. Feast, R.J. Peace, I.C. Sage, S. Till, E.L. Wood, Synthesis and device characterisation of side-chain polymer electron transport materials for organic semiconductor applications, J. Mater. Chem. 11 (2001) 2239–2244.

[12] J.L. Sessler, H. Maeda, T. Mizuno, V.M. Lynch, H. Furuta, Quinoxaline-bridged porphyrinoids, J. Am. Chem. Soc. 124 (2002) 13474–13479.

[13] H. Zhang, Y. Wu, W. Zhang, E. Li, C. Shen, H. Jiang, H. Tian, W.H. Zhu, Low cost and stable quinoxaline-based hole-transporting materials with a D-A-D molecular configuration for efficient perovskite solar cells, Chem. Sci. 9 (2018) 5919–5928.

[14] A. Renzoni, F. Zino, E. Franchi, Mercury levels along the food chain and risk for exposed populations, Environ. Res. 77 (1998) 68–72.

[15] O. Malm, Gold mining as a source of mercury exposure in the Brazilian Amazon, Environ. Res. 77 (1998) 73–78.

[16] Y. Zhang, M. Yang, C. Jia, M. Ji, Iodine-promoted domino oxidative cyclization for the one-pot synthesis of novel fused four-ring quinoxaline fluorophores by sp^3 C–H functionalization, Chem. Eur. J. 25 (2019) 13709–13713.

[17] S. Saha, B. Peña, K.R. Dunbar, Partially solvated dinuclear ruthenium compounds bridged by quinoxaline-functionalized ligands as Ru(II) photocage architectures for low-energy light absorption, Inorg. Chem. 58 (2019) 14568–14576.

[18] S.H. Afzali, A. Alzamly, R. Firouzi, I. Korobkov, S. Gambarotta, Radical chemistry of alkyl aluminum with quinoxaline ligands, J. Coord. Chem. 71 (2018) 1234–1249.

[19] A. Katoh, T. Yoshida, J. Ohkanda, Synthesis of Quinoxaline Derivatives Bearing the Styryl and Phenylethynyl Groups and Application to a Fluorescence Derivatization Reagent, Ci. Nii. Ac. Jp., 2000, pp. 911–920.

[20] G. Oberdörster, E. Oberdörster, J. Oberdörster, Nanotoxicology: an emerging discipline evolving from studies of ultrafine particles, Environ. Health Perspect. 113 (2005) 823–839.

[21] M.J. Crossley, L.A. Johnston, Laterally-extended porphyrin systems incorporating a switchable unit, Chem. Commun. 2 (2002) 1122–1123.

[22] M. Suresh, A.K. Mandal, S. Saha, E. Suresh, A. Mandoli, R. Di Liddo, P.P. Parnigotto, A. Das, Azine-based receptor for recognition of Hg^{2+} ion: crystallographic evidence and imaging application in live cells, Org. Lett. 12 (2010) 5406–5409.

[23] J. Ishikawa, H. Sakamoto, H. Wada, Synthesis and silver ion complexation behavior of fluoroionophores containing a benzothiazolyl group linked to an n-phenylpolythiazaalkane moiety, J. Chem. Soc. Perkin Trans. 2 (1999) 1273–1279.

[24] K. Rurack, M. Kollmannsberger, U. Resch-Genger, J. Daub, A selective and sensitive fluoroionophore for Hg(II), Ag(I), and CuII with virtually decoupled fluorophore and receptor units [10], J. Am. Chem. Soc. 122 (2000) 968–969.

[25] H. Rouh, Y. Liu, N. Katakam, L. Pham, Y.L. Zhu, G. Li, Synthesis of functionalized chromene and chroman derivatives via cesium carbonate promoted formal [4 + 2] annulation of 2′-hydroxychalcones with allenoates, J. Org. Chem. 83 (2018) 15372–15379.

[26] Y. Liu, S. Ahmed, X.Y. Qin, H. Rouh, G. Wu, G. Li, B. Jiang, Synthesis of diastereoenriched α-aminomethyl enaminones via a brønsted acid-catalyzed asymmetric aza-baylis-hillman reaction of chiral N-phosphonyl imines, Chem. Asian J. 15 (2020) 1125–1131.

[27] G. Wu, Y. Liu, Z. Yang, N. Katakam, H. Rouh, S. Ahmed, D. Unruh, K. Surowiec, G. Li, Multilayer 3D chirality and its synthetic assembly, Research 2019 (2019) 1–11.

[28] B. Wang, E.V. Anslyn, Chemosensors: Principles, Strategies, and Applications, John Wiley & Sons, Inc., Hoboken, NJ, USA, 2011.

[29] A.W. Czarnik, Chemical communication in water using fluorescent chemosensors, Acc. Chem. Res. 27 (1994) 302–308.

[30] B. Movassagh, H. Rooh, H.R. Bijanzadeh, A mild and highly efficient one-pot synthesis of 1,3,5-triaryl-2- pyrazolines, Chem. Heterocycl. Compd. 48 (2013) 1719–1721.

[31] S. Voutsadaki, G.K. Tsikalas, E. Klontzas, G.E. Froudakis, H.E. Katerinopoulos, A "turn-on" coumarin-based fluorescent sensor with high selectivity for mercury ions in aqueous media, Chem. Commun. 46 (2010) 3292–3294.

[32] A. Dhir, V. Bhalla, M. Kumar, Ratiometric sensing of Hg2+ based on the calix[4] arene of partial cone conformation possessing a dansyl moiety, Org. Lett. 10 (2008) 4891–4894.

[33] M.M. Yu, Z.X. Li, L.H. Wei, D.H. Wei, M.S. Tang, A 1,8-naphthyridine-based fluorescent chemodosimeter for the rapid detection of Zn^{2+} and Cu^{2+}, Org. Lett. 10 (2008) 5115–5118.

[34] R. Pandey, R.K. Gupta, M. Shahid, B. Maiti, A. Misra, D.S. Pandey, Synthesis and characterization of electroactive ferrocene derivatives: ferrocenylimidazoquinazoline as a multichannel chemosensor selectively for Hg 2+ and Pb^{2+} ions in an aqueous environment, Inorg. Chem. 51 (2012) 298–311.

[35] P. Das, A. Ghosh, H. Bhatt, A. Das, A highly selective and dual responsive test paper sensor of Hg $^{2+}$/Cr $^{3+}$ for naked eye detection in neutral water, RSC Adv. 2 (2012) 3714–3721.

[36] M. Update, Impact on Fish Advisories, EPA Fact Sheet EPA-823-F-01-011, 2001.

[37] W.C. Pfeiffer, L.D. Lacerda, W. Salomons, O. Malm, Environmental fate of mercury from gold mining in the Brazilian Amazon, Environ. Rev. 1 (1993) 26–37.

[38] P. Chu, D.B. Porcella, Mercury stack emissions from U.S. electric utility power plants, Water, Air, Soil Pollut. 80 (1995) 135–144.

[39] L. Wang, W.K. Wong, L. Wu, Z.Y. Li, A highly selective fluorescent chemosensor for Hg^{2+} in aqueous solution, Chem. Lett. 34 (2005) 934–935.

[40] E.M. Nolan, S.J. Lippard, A "turn-on" fluorescent sensor for the selective detection of mercuric ion in aqueous media, J. Am. Chem. Soc. 125 (2003) 14270–14271.

[41] T. Ahmadi, S. Bahar, G. Mohammadi Ziarani, A. Badiei, Formation of functionalized silica-based nanoparticles and their application for extraction and determination of Hg (II) ion in fish samples, Food Chem. 300 (2019), 125180.

[42] G. Shiravand, J.B. Ghasemi, A. Badiei, G. Mohammadi Ziarani, A dual-emission fluorescence probe for simultaneous quantification of CN^- and $Cr_2O_7^{2-}$ ions based on modified g-C_3N_4, J. Photochem. Photobiol. Chem. (2019), 112261.

[43] G. Mohammadi Ziarani, V. Fathi Vavsari, A. Badiei, J. Afshani, P. Gholamzadeh, S. Balalaie, F. Faridbod, M.R. Ganjali, A highly sensitive fluorescent bulk sensor based on isonicotinic acid hydrazide–immobilized nano-fumed silica (fumed-Si–INAH) for detection of Hg^{2+} and Cr^{3+} ions in aqueous media, J. Iran. Chem. Soc. 15 (2018) 211–221.

[44] T. Ahmadi, G. Mohammadi Ziarani, S. Bahar, A. Badiei, Domino synthesis of quinoxaline derivatives using SBA-Pr-NH_2 as a nanoreactor and their spectrophotometric complexation studies with some metals ions, J. Iran. Chem. Soc. 15 (2018) 1153–1161.

[45] E.V. Verbitskiy, Y.A. Kvashnin, A.A. Baranova, K.O. Khokhlov, R.D. Chuvashov, I.E. Schapov, Y.A. Yakovleva, E.F. Zhilina, A.V. Shchepochkin, N.I. Makarova, E.V. Vetrova, A.V. Metelitsa, G.L. Rusinov, O.N. Chupakhin, V.N. Charushin, Synthesis and characterization of linear 1,4-diazine-triphenylamine–based selective chemosensors for recognition of nitroaromatic compounds and aliphatic amines, Dye. Pigment. 178 (2020), 108344.

[46] S. Goswami, S. Chakraborty, M.K. Adak, S. Halder, C.K. Quah, H.-K. Fun, B. Pakhira, S. Sarkar, A highly selective ratiometric chemosensor for Ni^{2+} in a quinoxaline matrix, New J. Chem. 38 (2014) 6230–6235.

[47] Priyadip Das, Amrita Ghosh, Hitesh Bhatt, Amitava Das, A highly selective and dual responsive test paper sensor of Hg $^{2+}$/Cr^{3+} for naked eye detection in neutral water, RSC Adv. 2 (2012) 3714–3721.

[48] G. Wei, Z. Yan, J. Tian, G. Zhao, S. Guang, H. Xu, Efficient polymer pendant approach toward high stable organic fluorophore for sensing ultratrace Hg^{2+} with improved biological compatibility and cell permeability, Anal. Chem. 92 (2020) 3293–3301.

[49] M. Li, B. Li, L. Zhou, Y. Zhang, Q. Cao, R. Wang, H. Xiao, Fluorescence-sensitive adsorbent based on cellulose using for mercury detection and removal from aqueous solution with selective "on-off" response, Int. J. Biol. Macromol. 132 (2019) 1185–1192.

[50] C. Lu, P.J. Jimmy Huang, Y. Ying, J. Liu, Covalent linking DNA to graphene oxide and its comparison with physisorbed probes for Hg^{2+} detection, Biosens. Bioelectron. 79 (2016) 244–250.

[51] M.B. Gumpu, M. Veerapandian, U.M. Krishnan, J.B.B. Rayappan, Simultaneous electrochemical detection of Cd(II), Pb(II), As(III) and Hg(II) ions using ruthenium(II)-textured graphene oxide nanocomposite, Talanta 162 (2017) 574–582.

[52] H. Zhu, C. Han, Y.H. Li, G.H. Cui, Two new coordination polymers containing long flexible bis(benzimidazole) ligand as luminescent chemosensors for acetylacetone and Hg(II) ions detection, J. Solid State Chem. 282 (2020) 121132.

[53] L. Luo, P. Wang, Y. Wang, F. Wang, pH assisted selective detection of Hg(II) and Ag(I) based on nitrogen-rich carbon dots, Sensor. Actuator. B Chem. 273 (2018) 1640–1647.

[54] H.L. Yang, X.W. Sun, Y.M. Zhang, Z.H. Wang, W. Zhu, Y.Q. Fan, T.B. Wei, H. Yao, Q. Lin, A bi-component supramolecular gel for selective fluorescence detection and removal of Hg2+ in water, Soft Matter 15 (2019) 9547–9552.

[55] H.L. Min, B.K. Cho, J. Yoon, S.K. Jong, Selectively chemodosimetric detection of Hg(II) in aqueous media, Org. Lett. 9 (2007) 4515–4518.

[56] L. Li, B. Yu, T. You, Nitrogen and sulfur co-doped carbon dots for highly selective and sensitive detection of Hg (II) ions, Biosens. Bioelectron. 74 (2015) 263–269.

[57] M.R. Awual, M.M. Hasan, G.E. Eldesoky, M.A. Khaleque, M.M. Rahman, M. Naushad, Facile mercury detection and removal from aqueous media involving ligand impregnated conjugate nanomaterials, Chem. Eng. J. 290 (2016) 243–251.

[58] B.-C. Ye, B.-C. Yin, Highly sensitive detection of mercury(II) ions by fluorescence polarization enhanced by gold nanoparticles, Angew. Chem. 120 (2008) 8514–8517.
[59] S. Kraithong, W. Panchan, A. Charoenpanich, J. Sirirak, S. Sahasithiwat, P. Swanglap, V. Promarak, P. Thamyongkit, N. Wanichacheva, A method to detect Hg2+ in vegetable via a "Turn–ON" Hg^{2+} Fluorescent sensor with a nanomolar sensitivity, J. Photochem. Photobiol. Chem. 389 (2020), 112224.
[60] J.M.V. Ngororabanga, Z.R. Tshentu, N. Mama, A highly selective and sensitive ESIPT-based coumarin-triazole polymer for the ratiometric detection of Hg^{2+}, New J. Chem. 43 (2019) 12168–12177.
[61] Y. Liu, J. Zhang, T. Feng, Y. Li, Synthesis, structure-fluorescence relationships and density functional theory studies of novel naphthalimide-piperazine-pyridine-based polystyrene sensors for Hg(II) detection, RSC Adv. 10 (2020) 25281–25289.
[62] L. Huang, Z. Yang, Z. Zhou, Y. Li, S. Tang, W. Xiao, M. Hu, C. Peng, Y. Chen, B. Gu, H. Li, A dual colorimetric and near-infrared fluorescent turn-on probe for Hg^{2+} detection and its applications, Dye. Pigment. 163 (2019) 118–125.
[63] P.J.J. Huang, C. Van Ballegooie, J. Liu, Hg^{2+} detection using a phosphorothioate RNA probe adsorbed on graphene oxide and a comparison with thymine-rich DNA, Analyst 141 (2016) 3788–3793.
[64] C. Li, Q. Niu, J. Wang, T. Wei, T. Li, J. Chen, X. Qin, Q. Yang, Bithiophene-based fluorescent sensor for highly sensitive and ultrarapid detection of Hg^{2+} in water, seafood, urine and live cells, Spectrochim. Acta Part A Mol. Biomol. Spectrosc. 233 (2020), 118208.
[65] T.H. Nguyen, T. Sun, K.T.V. Grattan, A turn-on fluorescence-based fibre optic sensor for the detection of mercury, Sensors 19 (2019) 2142.
[66] S. Ruan, H. Ebendorff-Heidepriem, Y. Ruan, Optical fibre turn-on sensor for the detection of mercury based on immobilized fluorophore, Meas. J. Int. Meas. Confed. 121 (2018) 122–126.
[67] M. Darroudi, Y. Sarrafi, M. Hamzehloueian, Theoretical exploration of mechanism of carbapenam formation in catalytic Kinugasa reaction, Tetrahedron 73 (2017) 1673–1681.
[68] M. Darroudi, S. Ranjbar, M. Esfandiar, M. Khoshneviszadeh, M. Hamzehloueian, M. Khoshneviszadeh, Y. Sarrafi, Synthesis of novel triazole incorporated thiazolone motifs having promising antityrosinase activity through green nanocatalyst CuI-Fe_3O_4@SiO_2 (TMS-EDTA), Appl. Organomet. Chem. (2020). In press.
[69] M. Darroudi, Y. Sarrafi, M. Hamzehloueian, An efficient synthesis of novel triazoles incorporating barbituric motifs via [3+2] cycloaddition reaction: experimental and theoretical study, J. Serb. Chem. Soc. 83 (2018) 821–835.
[70] N. Lashgari, A. Badiei, G. Mohammadi Ziarani, Modification of mesoporous silica SBA-15 with different organic molecules to gain chemical sensors : a review, Nano. Chem. Res. 1 (2016) 127–141.
[71] N. Lashgari, A. Badiei, G. Mohammadi Ziarani, F. Faridbod, Isatin functionalized nanoporous SBA-15 as a selective fluorescent probe for the detection of Hg(II) in water, Anal. Bioanal. Chem. 409 (2017) 3175–3185.
[72] M. Karimi, A. Badiei, N. Lashgari, J. Afshani, G. Mohammadi Ziarani, A nanostructured LUS-1 based organic-inorganic hybrid optical sensor for highly selective sensing of Fe^{3+} in water, J. Lumin. 168 (2015) 1–6.
[73] G. Mohammadi Ziarani, N. Lashgari, A. Badiei, Sulfonic acid-functionalized mesoporous silica (SBA-Pr-SO_3H) as solid acid catalyst in organic reactions, J. Mol. Catal. Chem. 397 (2015) 166–191.
[74] D. Zhao, Q. Huo, J. Feng, B.F. Chmelka, G.D. Stucky, Nonionic triblock and star diblock copolymer and oligomeric sufactant syntheses of highly ordered, hydrothermally stable, mesoporous silica structures, J. Am. Chem. Soc. 120 (1998) 6024–6036.
[75] G. Mohammadi Ziarani, A.R. Badiei, Y. Khaniania, M. Haddadpour, One pot synthesis of polyhydroquinolines catalyzed by sulfonic acid functionalized SBA-15 as a new nanoporous acid catalyst under solvent free conditions, Iran. J. Chem. Eng. 29 (2) (2010) 1–10.
[76] G. Mohammadi Ziarani, A. Badiei, M. Haddadpour, Application of sulfonic acid functionalized nanoporous silica (SBA-Pr-SO_3H) for one-pot synthesis of quinoxaline derivatives, Int. J. Chem. 3 (2011) 87–94.
[77] M.J. Frisch, G.W. Trucks, H.B. Schlegel, G.E. Scuseria, M.A. Robb, J.R. Cheeseman, G. Scalmani, V. Barone, B. Mennucci, G.A. Petersson, H. Nakatsuji, M. Caricato, X. Li, H.P. Hratchian, A.F. Izmaylov, J. Bloino, G. Zheng, J.L. Sonnenberg, M. Hada, M. Ehara, K. Toyota, R. Fukuda, J. Hasegawa, M. Ishida, T. Nakajima, Y. Honda, O. Kitao, H. Nakai, T. Vreven, J. Montgomery, J. A, J.E. Peralta, F. Ogliaro, M. Bearpark, J.J. Heyd, E. Brothers, K.N. Kudin, V.N. Staroverov, R. Kobayashi, J. Normand, K. Raghavachari, A. Rendell, J.C. Burant, S.S. Iyengar, J. Tomasi, M. Cossi, N. Rega, J.M. Millam, M. Klene, J.E. Knox, J.B. Cross, V. Bakken, C. Adamo, J. Jaramillo, R. Gomperts, R.E. Stratmann, O. Yazyev, A.J. Austin, R. Cammi, C. Pomelli, J.W. Ochterski, R.L. Martin, K. Morokuma, V.G. Zakrzewski, G.A. Voth, P. Salvador, J.J. Dannenberg, S. Dapprich, A.D. Daniels, Ö. Farkas, J.B. Foresman, J.V. Ortiz, J. Cioslowski, D.J. Fox, Gaussian 09, revision A. http://www.gaussian.com/g_tech/g_ur/m_citation.htm, 2009. (Accessed 21 December 2016).
[78] C. Gonzalez, H.B. Schlegel, An improved algorithm for reaction path following, J. Chem. Phys. 90 (1989) 2154–2161.
[79] C. Gonzalez, H.B. Schlegel, Reaction path following in mass-weighted internal coordinates, J. Phys. Chem. 94 (1990) 5523–5527.
[80] A. Klamt, G. Schüürmann, COSMO: a new approach to dielectric screening in solvents with explicit expressions for the screening energy and its gradient, J. Chem. Soc., Perkin Trans. 2 (1993) 799–805.
[81] J. Andzelm, C. Kolmel, A. Klamt, Incorporation of solvent effects into density functional calculations of molecular energies and geometries, J. Chem. Phys. 103 (1995) 9312–9320.
[82] V. Barone, M. Cossi, Quantum calculation of molecular energies and energy gradients in solution by a conductor solvent model, J. Phys. Chem. A. 102 (1998) 1995–2001.
[83] M. Cossi, N. Rega, G. Scalmani, V. Barone, Energies, structures, and electronic properties of molecules in solution with the C-PCM solvation model, J. Comput. Chem. 24 (2003) 669–681.
[84] S. Grimme, Semiempirical GGA-type density functional constructed with a long-range dispersion correction, J. Comput. Chem. 27 (2006) 1787–1799.
[85] M. Rahm, T. Brinck, Novel 1,3-dipolar cycloadditions of dinitraminic acid: implications for the chemical stability of ammonium dinitramide, J. Phys. Chem. A. 112 (2008) 2456–2463.
[86] K.V. Gothelf, K.A. Jørgensen, Asymmetric 1,3-dipolar cycloaddition reactions, Chem. Rev. 98 (1998) 863–910.
[87] D.M. Andrada, A.M. Granados, M. Solà, I. Fernández, DFT study of thermal 1,3-dipolar cycloaddition reactions between alkynyl metal(0) fischer carbene complexes and 3 H-1,2-dithiole-3-thione derivatives, Organometallics 30 (2011) 466–476.
[88] Z. Chen, L. Lin, M. Wang, X. Liu, X. Feng, Asymmetric synthesis of trans-β-lactams by a Kinugasa reaction on water, Chem. Eur J. 19 (2013) 7561–7567.